HiSST: 3rd International Conference on
High-Speed Vehicle Science Technology
14 -19 April 2024, Busan, Korea

# Experimental Investigation of Combustion Mode Transitions in a Cavity-based Scramjet

*Le Li[1], Jiajian Zhu[2]*,Minggang Wan[3]*, Yifu Tian[4], Tiangang Luo[5], Qinyuan Li[6], Shuaijia Shao[7], Mingbo Sun[8]*

## Abstract

This work aimed to investigate combustion mode transitions in a cavity-based scramjet combustor. The experiments were carried out on a direct-connected facility with an inflow condition of Mach number 2.52, total pressure of 1.35 MPa, total temperature of 1650 K and total flow rate of 1 kg/s. The fuel injector consisted of two injection ports: fuel was continuously injected from one port while the other controlled the fuel flow for mode transitions by switching it on or off. High-speed schlieren and CH* imaging were used to characterize the dynamics of combustion mode transitions. Results showed that the back pressure in the scramjet combustor rose with the increasing combustion heat release, causing the oblique shock wave in supersonic combustion mode to shorten and move forward. Then an oblique shock train was formed above the cavity, marking it as a dual-mode supersonic combustion mode. As the back pressure continued to rise, the shock train was expelled from the combustor, indicating a subsonic combustion mode. During this process, the flame was intensified and shifted upstream, transitioning from shear-layer stabilization to jet-wake stabilization. The mode transition was accompanied by shock and flame oscillations. In the supersonic-to-dual transition, the reflected shock wave oscillated above the cavity. In the dual-to-supersonic transition, the oblique shock wave at the injection position alternately appeared and disappeared, causing the shock train to weaken and strengthen repeatedly. When the transition occurs between the dual combustion mode and the subsonic combustion mode, the shock train oscillated in the upper left corner of the field of view, with the combustor alternating between shock train and non-shock states. The flame heat release zone underwent cycles of merging and decomposing during these transitions. In addition, it was observed that suddenly increasing the fuel injection could temporarily suppress the combustion.

**Keywords**: *scramjet, cavity, mode transition, CH*, schlieren*

[1] *National University of Defense Technology, China, 14786658927@163.com*
[2] *National University of Defense Technology, China, jjzhu@nudt.edu.cn*
[3] *National University of Defense Technology, China, wanminggang18@nudt.edu.cn*
[4] *National University of Defense Technology, China, tianyifu@nudt.edu.cn*
[5] *National University of Defense Technology, China, luotiangang@nudt.edu.cn*
[6] *National University of Defense Technology, China, liqinyuan@nudt.edu.cn*
[7] *National University of Defense Technology, China, shaoshuaijia@nudt.edu.cn*
[8] *National University of Defense Technology, China, sunmingbo@nudt.edu.cn*

## 1. Introduction

The hypersonic vehicle, characterized by its exceptional flight speed and robust penetration capabilities, represents a strategic high-precision technology that is poised to revolutionize the nature and conduct of future warfare, thus assuming a pivotal strategic role for military powers globally [1]. Within the realm of hypersonic vehicles, the scramjet stands as the most promising power plant and core technological component, enabling atmospheric flight at hypersonic speeds. Numerous nations have dedicated significant resources to its research and development, leading to notable advancements in ignition and flame stabilization techniques [2-6]. However, despite these achievements, the optimization of scramjet performance remains a challenging endeavor, particularly pertaining to the seamless transition between combustion modes. This transition problem is recognized as a crucial aspect in the study of combustion modes, both domestically and internationally, and its resolution holds immense significance in the advancement of hypersonic technology [7].

Previous studies on combustion modes have primarily concentrated on elucidating the flame distribution and flow field characteristics within the combustor across various operational modes. Typically, in a single ignition experiment, the combustor remains fixed within a specific combustion mode. For instance, numerous scholars [8-12] have observed the flame's extent and brightness characteristics within the combustor at different equivalence ratios, categorizing the combustion mode into weak and strong combustion modes. Kobayashi et al. [13] measured the pressure on both sides of the wall during a combustion experiment. It was discovered that, in ramjet mode, the wall pressure distribution on both sides exhibited remarkable similarity, indicative of a uniform subsonic flow within the flow channel. Conversely, in scramjet mode, the wall pressure distribution manifested asymmetry, with the pressure on the fuel injection side exhibiting relative smoothness, while the pressure along the sidewall exhibited a zigzag pattern, characteristic of supersonic flow. Li et al. [14] employed a diverse array of measurement techniques to investigate the combustion mode. Multiple measurement sections were strategically positioned at the combustor inlet, as well as upstream and downstream of the intense heat release zone. Concurrently, the two-dimensional distribution of airflow static temperature, component partial pressure, and airflow velocity across multiple sections were measured under varying equivalence ratios. This approach allowed for the derivation of heat release distribution patterns and related characteristic parameter distributions within the combustor flow field under different modes. In a separate experiment, Wang et al. [15] conducted an investigation by injecting hydrogen upstream of the cavity. This enabled the observation of flame position distribution within the combustor under varying cavity structures, fuel injection schemes, and equivalence ratios. Based on these observations, they summarized three distinct flame stabilization modes that occur under different combustion modes: cavity assisted jet-wake stabilization, cavity shear-layer stabilization, and combined cavity shear-layer/recirculation stabilization. This comprehensive approach provides a deeper understanding of the intricate interactions between combustion modes within the combustor.

However, there exist pronounced differences in the aerodynamic characteristics and combustion modes of the engine when operating in sub-combustion and super-combustion modes [16]. These disparities may give rise to the instability of the aircraft's aerodynamic performance and abrupt variations in engine thrust. Consequently, numerous scholars have conducted pertinent research on the mode transition process. Fotia and Driscoll [17] employed pressure measurement techniques and high-speed laser interferometry to conduct ramjet-to-scramjet transition experiments on a direct-connected model scramjet experimental facility. During these experiments, the laser interference image sampling rate was maintained at 1 kHz, while the camera exposure time was set to 2 μs. By gradually decreasing the fuel flow rate, rapidly varying the fuel flow rate and test-section wall temperature, they successfully achieved the mode transition and derived the state diagram of the ramjet-to-scramjet transition boundary. Their findings revealed that under certain conditions, periodic low-frequency oscillations of the flame position occur, which are attributed to the oscillation of the upstream pre-combustion shock train. This phenomenon is caused by a self-sustaining instability

within the shear layer. In another study, Zhou et al. [18] utilized OH* spontaneous emission imaging (with a frame rate of 5 Hz and an exposure time of 150 ms), schlieren imaging (with a frame rate of 800 Hz and an exposure time ranging from 3-10 μs), and wall static pressure sensors (operating at 25 Hz) to investigate the combustion mode and instability characteristics of the scramjet. This comprehensive approach enabled them to analyze the fundamental operating parameters and trigger mechanisms associated with acceleration-induced mode transition. Aguilera and Yu [19] discovered that during the scramjet-to-ramjet transition, a sequence of flame oscillations, encompassing transient thermal choking, flame flashback, cavity flame holding, and detachment, were triggered by mode hopping cycles. Furthermore, these mode hopping cycles were themselves instigated by thermal choking. Employing high-speed schlieren imaging techniques (with a frame rate of 6000 fps and an exposure time of 2 μs), along with CH* spontaneous emission imaging (at a frame rate of 6000 fps and an exposure time of 20 μs), Lian et al. [20] conducted ground-based direct-connection tests simulating transient acceleration and deceleration within the flight Mach number range of 5 ~ 6. Lian's team hypothesized that the synchronization of total heat release and the internal flow channel plays a pivotal role in governing both the mode transition and the thrust abruption process. Additionally, the flow characteristics were primarily influenced by the evolution of the pre-combustion shock wave within the isolator. In a separate study, Zhang et al. [21] observed the thrust hysteresis effect in their investigation of mode transitions.

Currently, the experiment of combustion mode transition faces several challenges, including the limited sampling frequency and extended exposure time associated with spontaneous emission imaging techniques. The majority of research efforts have been concentrated on the scramjet-to-ramjet transition process, leaving the intermediate mode underexplored. In light of these issues, the present study introduces a direct-connected scramjet combustor test bench using synchronized, high-speed schlieren and CH* imaging with a frequency of 10 kHz. This work is focused on the mode transition processes in the combustor. This analysis provides a deeper understanding about the flow field and flame characteristics during the transitions.

## 2. Experimental setup

The experiment was conducted at the direct-connection scramjet facility of the National University of Defense Technology. This facility comprises an air heater, a Mach 2.52 Laval nozzle, a scramjet combustor, a fuel supply system, and a measurement control system. The air heater utilizes the combustion of a mixture of pure oxygen, pure alcohol, and air within a circular cross-section combustor, employing water-cooled thermal protection to heat the air. Subsequently, the heated air is accelerated to a supersonic state through a rectangular cross-section nozzle. The simulation of supersonic incoming flows at varying flight altitudes is achieved by adjusting the proportions of these three components. The heater terminates in a transition from a round to a square shape, facilitating the connection to the rectangular nozzle. The design of the nozzle is founded on the characteristic line method, with corrections made to account for the influence of the boundary layer. During this experiment, the heater generated a high-enthalpy airflow, maintaining the mass flow rate of approximately 1 kg/s, the total pressure of 1.35 MPa, and the total temperature of 1650 K. This heated airflow was further accelerated through the rectangular cross-section nozzle, ultimately entering the model combustor at a Mach number of 2.52.

The diagnostic system selects both wall pressure measurements and optical measurements, tailored to meet the specific experimental requirements. This selection encompasses the PSI pressure scanning valve, the CH* spontaneous emission imaging system, the schlieren imaging system, among others. The aforementioned diagnostic approach enables precise measurements of heat release distribution, flow field structure, and dynamic characteristics within the scramjet combustor. Furthermore, the measurement technique employed is both mature and efficient, ensuring reliable and accurate data acquisition.

The upper and lower walls of the isolator, as well as those of the test bench's isolator, are designed with pressure measuring holes, each measuring 1 mm in diameter. For pressure measurements, the Pressure System Inc. 9116 pressure scanning valve is utilized. This valve comprises a control module and a measurement module, the latter boasting 16 measurement channels. The pressure signal sampling frequency stands at 100 Hz, with a measurement range of 100 atm and a measurement accuracy of 0.05%. The CH* spontaneous emission imaging system comprises a 430±10 nm CH*

filter, an EyeiTS HI-QE Blue single-layer image intensifier, and a SSZN SH6-113 high-speed camera. The sampling frequency of this system is 10 kHz, while the exposure time is set at 2 μs, ensuring rapid and sensitive capture of optical emissions. The schlieren device employs a standard Z-type configuration and collaborates with the ISSI LMS LED light source and the NAC Memrecam GO-12 intelligent high-speed camera system to capture schlieren images. The sampling frequency is set at 10 kHz, with an exposure time of 1.1 μs. The synchronous imaging of CH* spontaneous emission and schlieren is achieved through the timing synchronization controller DG 645. The pressure measurement system, CH* spontaneous emission imaging high-speed photography camera, image intensifier, and schlieren high-speed photography camera are all triggered by DG 645 and the PXI control system of the direct connection station's main body. This triggering is executed in accordance with the operational instructions provided by the experimental console, ensuring the synchronization of equipment operation and measurement timing. The schematic representation of the test system is presented in Fig. 1.

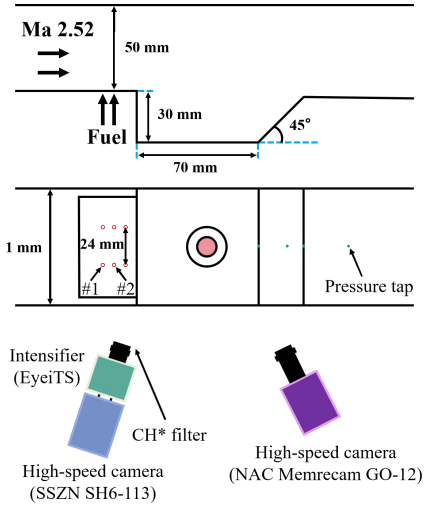


**Fig. 1** Experimental system diagram

This work on mode transition focuses primarily on the combustion state within the combustor. Based on the shock wave structure and heat release intensity within the combustor flow field, the combustion mode is categorized into supersonic combustion mode, dual-mode supersonic combustion mode (hereinafter referred to as dual combustion mode for brevity), and subsonic combustion mode [22]. It should be noted that in this article, the mode after the shock train is pushed away from the combustor is defined as subsonic combustion mode, and no further subdivision is made based on the shock wave pattern in the isolator. The distinct characteristics of each mode will be elucidated in detail at the outset of the third section.

**Table 1** Test condition table

| Test condition | $C_2H_4$ flow g/s (Phase I) | $C_2H_4$ flow g/s (Phase II) | $C_2H_4$ flow g/s (Phase III) | Mode transition path |
|---|---|---|---|---|
| Case A | 18.3 | - - | 61.3 | supersonic-to-subsonic |
| Case B | 18.3 | 39.6 | 11.9 | supersonic-to-dual-to-supersonic |
| Case C | 39.6 | 64.1 | 25.8 | Dual-to-subsonic-to-dual |

In the initial phase of the experiment, the combustion mode was established based on a predefined equivalence ratio. Specifically, for an equivalence ratio below 0.4, the combustor operated in the supersonic combustion mode. Within the range of an equivalence ratio greater than 0.4 but less than 0.7, the operation was classified as dual combustion mode. Conversely, when the equivalence ratio exceeded 0.7, the combustor functioned in subsonic combustion mode. The transition between these modes in the combustor was regulated by manipulating the injection pressure and timing of the two fuel supply lines. The high-speed camera commenced shooting at time zero, and the downstream

injection (#2) pipeline valve opened at −300 ms. In case A, the upstream injection (#1) pipeline valve was opened subsequent to 200 ms, and both injection valves were closed simultaneously after 1050 ms. In case B and C, the #1 solenoid valve was opened at 100 ms and closed at 450 ms, with the final closure of the #2 solenoid valve occurring at 1050 ms. The experimental conditions, including the specific parameters utilized for these manipulations, are detailed in Table 1.

## 3. Results and discussion

By analyzing the flow field structure and heat release distribution within the combustor across diverse operating conditions, the characteristics of the combustion mode transition within the flow field have been comprehensively summarized. Furthermore, the underlying mechanism responsible for the transition of combustion modes has been elucidated. Representative flow field images depicting the supersonic combustion mode, dual combustion mode, and subsonic combustion mode were selected from the experimental dataset. Subsequently, a total of 500 consecutive images were chosen for time-average processing, as illustrated in Fig. 2.

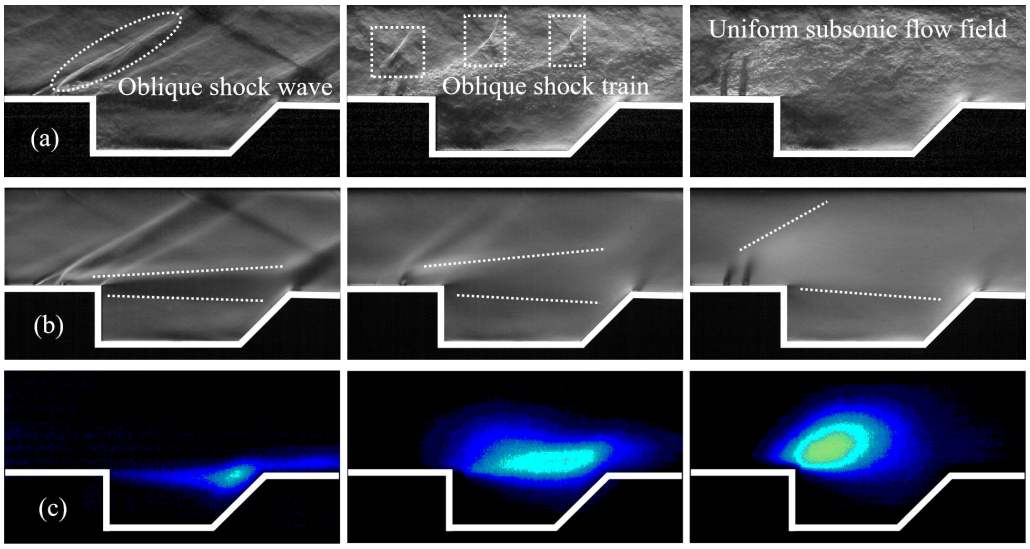


**Fig. 2** The instantaneous (a) and time-averaged images of schlieren (b) and CH* spontaneous emission (c) under supersonic combustion (left), dual combustion(center) and subsonic combustion (right) mode. The white dotted line demarcates the boundary of the transverse jet mixing layer.

In the supersonic combustion mode, the inlet of the combustor is characterized by a supersonic airflow, which interacts with the transverse fuel jet to generate an oblique shock wave, evident in the left panel of Fig. 2. Under these conditions, the flame within the combustor exhibits a flat and weak profile, indicative of a shear-layer stabilization, with the intense heat release zone concentrated at the cavity slope. The dual combustion mode also maintains a supersonic airflow at the combustor inlet. However, due to an increase in fuel quantity, the heat release within the combustor is significantly enhanced, resulting in excessive back pressure. Consequently, an oblique shock train forms within the isolator and combustor. This shock train migrates upstream, accompanied by small-scale oscillations, rendering a distinct oblique shock train structure indistinct after time-averaging. Nevertheless, it is observable that the transverse jet mixing layer is thicker compared to the supersonic combustion mode. Additionally, the flame thickness and intensity are notably augmented, with the primary heat release zone situated above the cavity. Lastly, in the subsonic combustion mode, the heat release from combustion further intensifies, leading to a continued increase in back pressure. Consequently, the shock train is expelled from the combustor, resulting in a uniform subsonic flow field in the combustor that is non-shock state.

### 3.1. Supersonic-to-subsonic transition

The initiation of the high-speed camera's recording coincided with the supersonic combustion mode of the combustor, where the flame stabilization manifested as shear-layer stabilization. At 200 ms, the solenoid valve of the upstream injection pipeline was actuated, initiating a gradual increase in fuel quantity. Fig. 3 illustrates that at 279.9 ms, the fuel ejected from the injection orifice mingled with the incoming airflow, generating a shock wave. Due to the added fuel absorbing heat in the

combustor, a temporary combustion suppression occurred. At 287.6 ms, the first reflected shock wave began to compress, leading to an enhancement of the flame. Subsequently, at 294.6 ms, the high-density region (depicted as black) behind the cavity slope disappeared, as the second reflected shock wave migrated from the downstream into the field of view and continued to propagate forward. This shift was accompanied by a rise in the flame tail. As the process continued, the first reflected shock wave further compressed, gradually reducing the distance between the two reflected shock waves. By 299.9 ms, the two reflected shock waves had converged, lifting the flame tail further and intensifying the region of strong heat release. At 306.7 ms, the reflected shock wave attained a length comparable to the thickness of the black area observed on the upper right, with a portion of the flame penetrating into the cavity, thereby expanding the flame area.

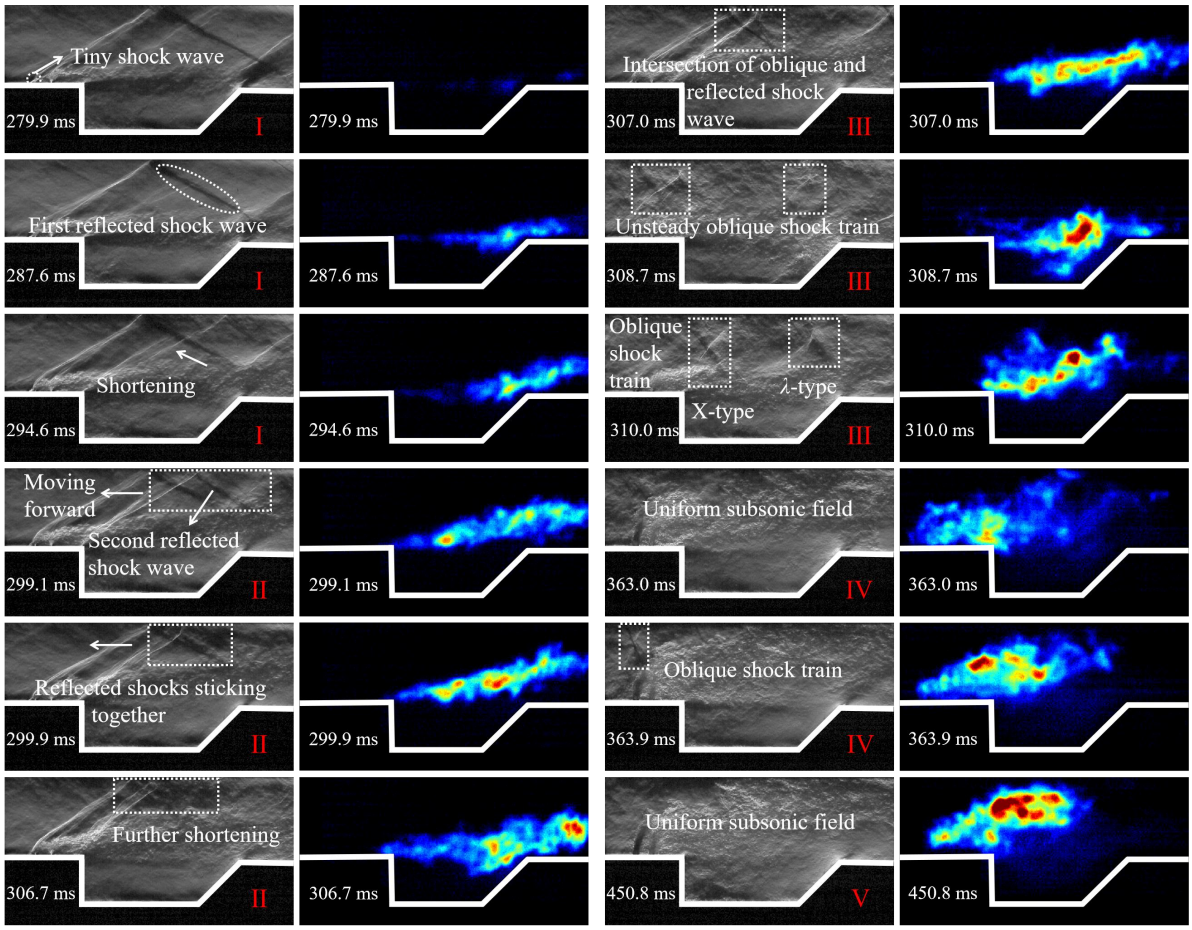


**Fig. 3** Instantaneous image of supersonic-to-subsonic transition process. In the phase I, the first reflected shock wave moved forward and shortened, resulting in an enhancement of the flame. In the phase II, the distance between the two reflected shock waves decreased and they moved forward together. The flame expanded into the cavity. In the phase III, the oblique shock wave intersected with the reflected shock wave, initiating the formation of the oblique shock train. In the phase IV, the oblique shock train moved forward and oscillated, with the dual combustion mode and the subsonic combustion mode repeatedly converting between each other, ultimately stabilizing in the subsonic combustion mode.

At 307 ms, a fully developed oblique shock train structure emerged above the combustor and began migrating upstream. Concurrently, the region experiencing intense flame heat release shifted towards the leading edge of the cavity. At 308.7 ms, the shock wave structure exhibited instability, with the flame heat release area concentrating above the cavity slope. The flame stabilization remained as the shear-layer stabilization. By 310 ms, the oblique shock train with its complete structure reappeared above the combustor, facilitating the flame's propagation forward to the upstream of the cavity. The region of intense flame heat release also advanced. As fuel supply increased, the oblique shock train advanced further.

At 363.0 ms, the oblique shock train exited the field of view, resulting in a thickening and further upstream advancement of the flame. The intense heat release zone of the flame shifted above the leading edge of the cavity. At 363.9 ms, the oblique shock train reentered the field of view, leading to an increase and concentration of the flame's intense heat release zone near the cavity's leading edge. After several alternating appearances of the oblique shock train and non-shock states within the field of view, the combustor stabilized in the subsonic combustion mode at 450.8 ms. At this point, the flame thickness approximated the height of the mainstream channel, with the intense heat release zone situated within the mainstream area above the cavity.

The entire mode transition process can be systematically categorized into five distinct phases. Phase I: The upstream injection hole initiates fuel jet, generating a minor shock wave. Subsequently, the first reflected shock wave begins to shorten and propagate forward. During this phase, the combustor's flame stabilization occurs primarily in the shear-layer stabilization, with the tail of the flame adhering to the cavity slope.

Phase II: As the quantity of fuel increases, there is a corresponding elevation in heat release, leading to an augmentation in back pressure within the combustor. Consequently, the reflected shock wave migrates upstream while continuously shortening. Additionally, the distance between the two reflected shock waves continuously decreases. Notably, the tail of the flame ascends, and a minor portion of the flame ingress into the cavity.

Phase III: The reflected shock wave proceeds forward and intersects with the oblique shock wave emanating from the fuel injection point. Notably, the shock wave at the injection site experiences a marked weakening. Following the initial transient period of instability, an oblique shock train emerges, exhibiting consistent forward motion interspersed with minor oscillations. Within the combustor, the flame stabilization mechanism transitions from the shear-layer stabilization to the combined cavity shear-layer/recirculation stabilization, ultimately initiating a shift towards the jet-wake stabilization.

Phase IV: The heat release within the combustor continues to escalate, concurrent with the onward progression of the oblique shock train. This shock train exhibits limited oscillatory behavior, confined to a narrow region in the upper left quadrant of the combustor. Significantly, the size of the shock train diminishes considerably, ultimately leading to its expulsion from the observation field. Simultaneously, the flame advances upstream, towards the leading edge of the cavity, and the flame stabilization is jet-wake stabilization.

Phase V: The oblique shock train is expelled from the observation field and, upon migrating to the isolator, transforms into either a normal or quasi-normal shock train. Within the combustor, the absence of shock waves gives rise to a uniform subsonic flow field. Under these conditions, both the flame thickness and heat release intensity attain peak values.

### 3.2. Dual-to-supersonic transition

In the preceding article, the flow field characteristics pertaining to the transition from the supersonic combustion mode to the dual combustion mode have been thoroughly delineated. Consequently, Case B primarily focuses on the analysis of the flow field and heat release characteristics during the reversal from the dual combustion mode back to the supersonic combustion mode.

As depicted in Fig. 4, after a duration of 231.3 ms, an oblique shock train emerged within the mainstream, exhibiting continuous forward motion interspersed with minor oscillations. Notably, the intense heat release zone of the flame was situated above the cavity, with a portion of the flame extending upstream towards the leading edge of the cavity. Subsequently, at 450 ms, the solenoid valve regulating the fuel supply pipeline leading to the upstream injection was deactivated. By 524.4 ms, a reduction in fuel supply had resulted in a diminished structural size and intensity of the oblique shock train within the observation field. Meanwhile, the tail of the flame lifted, and the zone of intense heat release shifted forwards towards the front of the cavity.

Shortly after, at 524.5 ms, a prominent oblique shock wave materialized proximal to the upstream injection, leading to a further weakening of the shock train situated above the combustor. At 524.6 ms, the oblique shock wave near the upstream injection dissipated into several smaller shock waves, while the structure of the shock train above became more prominent. Concurrently, the flame expanded along the flow direction, and the zone of intense heat release retreated. By 524.7 ms, both the shock wave and heat release zone had weakened significantly. Notably, the strong heat release

zone split into two distinct regions, one situated in front of the cavity and the other behind it. At 524.8 ms, the oblique shock wave proximate to the upstream injection vanished, revealing a clearer structure of the oblique shock train. Over repeated observations, it was noted that the duration of the oblique shock wave's persistence near the upstream injection increased, and the strong heat release zone polymerized again.

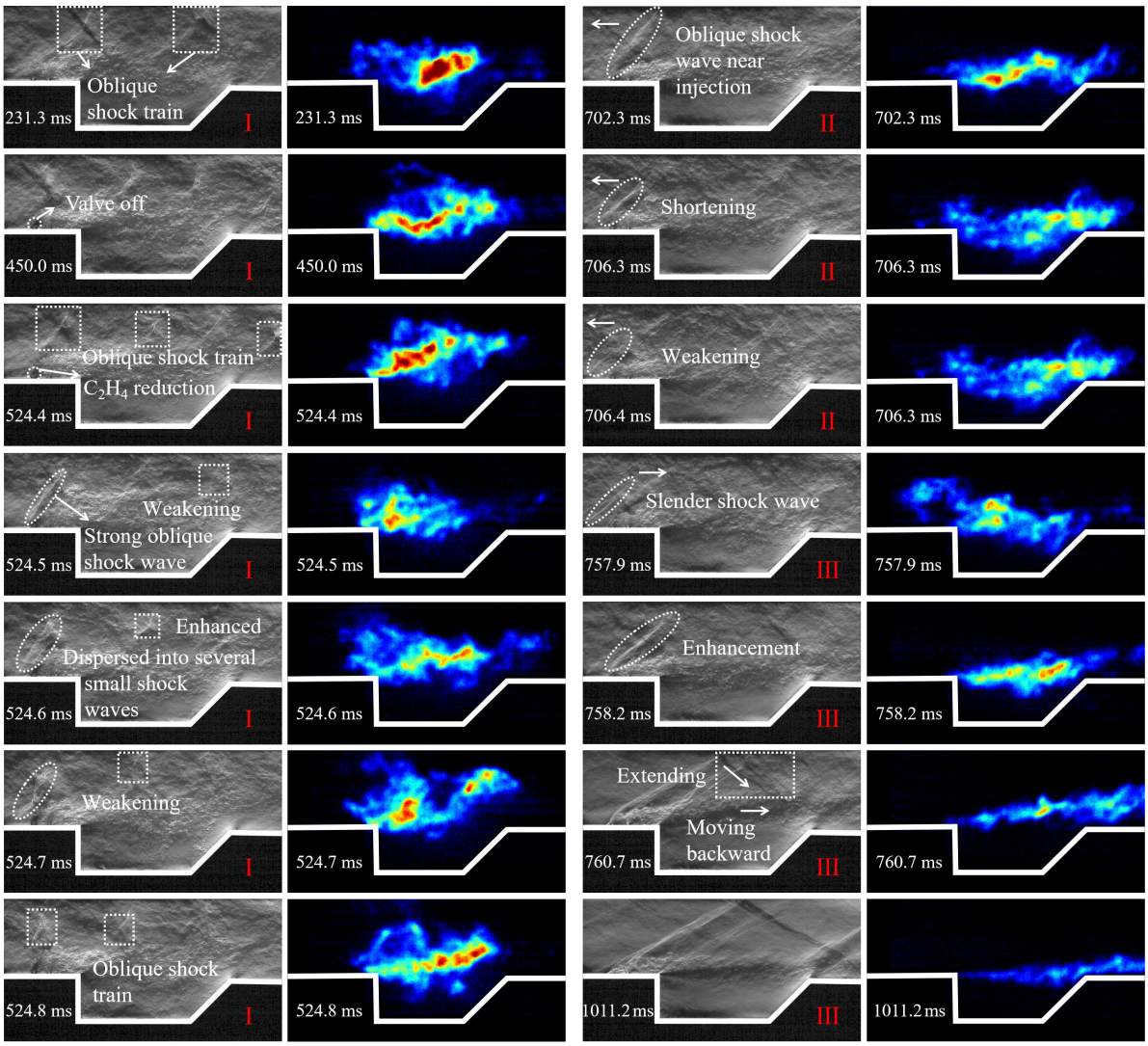


**Fig. 4** Instantaneous image of dual-to-supersonic transition process. Initially, the intensity of the oblique shock train diminished, with intermittent, yet fleeting, occurrences of a prominent oblique shock wave upstream of the jet. Progressing to the second phase, the duration of the oblique shock wave's presence upstream of the jet increased, observable as it migrated further upstream. Finally, in the third phase, the oblique shock wave surrounding the injection point intensified, extending towards the apex of the combustor to form a reflected shock wave, thereby indicating the transition of the combustor into the supersonic combustion mode.

Between 702.3 ms and 706.4 ms, a distinct shock wave emerged above the injection, subsequently advancing and vanishing from the field of view. The flame flattened slightly, its intensity waned, and it extended into the cavity. At 757.9 ms, a slender shock wave commenced to manifest upstream of the injection. By 758.2 ms, this shock wave intensified and elongated, with the reflected shock wave commencing its downstream motion. At 760.7 ms, the shock wave emanating from the injection reached the top of the combustor, while the reflected shock wave descended to the midpoint of the cavity's bottom and continued its downstream progress. Ultimately, the first reflected shock wave oscillated stably at a position ranging from 2 ~ 10 mm downstream of the midpoint of the cavity's bottom, while the second reflected shock wave descended and disappeared from the field of view.

The entire mode transition process can be systematically categorized into four distinct phases. Phase I: As the fuel supply diminishes, the intensity of the oblique shock train wanes. Occasional oblique shock waves emerge near the upstream region of the injection, but these dissipate rapidly. As the frequency of these occurrences increases, the duration of their persistence elongates. The flame stabilization is shear-layer stabilization.

Phase II: The persistence of the oblique shock wave proximate to the upstream of the injection becomes significantly prolonged. Concurrently, the structure of the oblique shock train above the combustor gradually dissipates. Over time, the oblique shock wave shortens and weakens forward. The flame stabilization mechanism is converted to the combined cavity shear-layer/recirculation stabilization.

Phase III: The oblique shock wave near the upstream of the injection intensifies and extends towards the apex of the combustor. Upon reaching the top, a reflected shock wave is generated. This reflected shock wave continues to propagate until it reaches the wall of the flow channel, indicating a stable supersonic combustion mode within the combustor. The flame stabilization transforms into a shear-layer stabilization.

### 3.3. Subsonic-dual transition

The characteristics of the flow field during the transition from the dual combustion mode to the subsonic combustion mode have been exhaustively described in a previous article. Therefore, Case C primarily focuses on analyzing the flow field and heat release characteristics associated with the return of the subsonic combustion mode to the dual combustion mode. Fig. 5 illustrates that at 250.6 ms, the shock wave structure within the combustor disappeared. Subsequently, as the fuel supply decreased, an oblique shock train structure emerged on the upper left side of the combustor at 610.5 ms. However, the intense heat release zone of the flame promptly collapsed (at 610.6 ms and 610.7 ms) and relocated near the leading edge of the cavity.

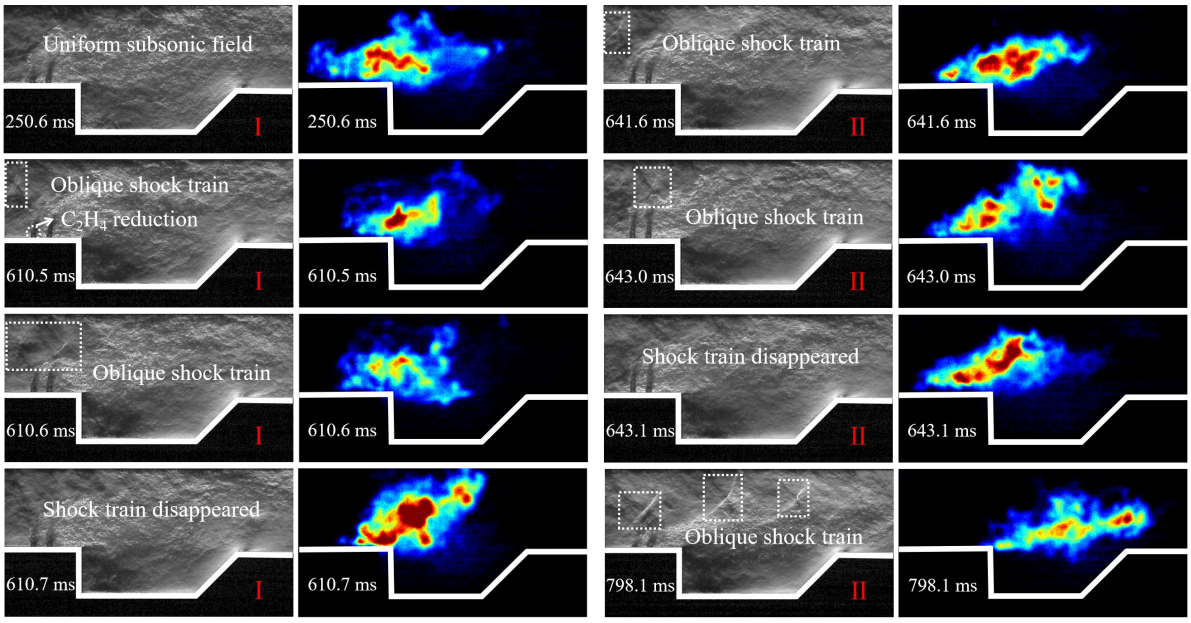


**Fig. 5** Instantaneous image of subsonic-to-dual transition process. In the initial phase, the oscillation amplitude of the oblique shock train remained minimal, with intermittent appearances in the upper left corner of the combustor. Progressing to the second phase, the heat release diminished further, resulting in an extended duration of the oblique shock train within the field of view. Additionally, a notable increase in the backward distance was observed, ultimately leading to the transition of the combustor into the dual combustion mode.

After several repeated occurrences, as the fuel quantity further diminished, the duration of the oblique shock train's maintenance gradually increased (from 641.6 ms to 643.0 ms), culminating in a return to a non-shock state at 643.1 ms. Within the combustor, a continuous transition persisted between the oblique shock train structure and the non-shock state, albeit with a prolonged existence

of the oblique shock train. Finally, at 798.1 ms, an oblique shock train exhibiting continuous oscillations persisted above the combustor, indicating a stable dual combustion mode.

The entire mode transition process can be categorized into two distinct phases. Phase I: as fuel diminishes, the back pressure within the combustor decreases, resulting in the downstream migration of the shock train structure. Occasionally, an oblique shock train emerges in the upper left corner of the combustor, but it is promptly repelled and exits the field of view. The flame stabilization is jet-wake stabilization.

Phase II: the oblique shock train continues to migrate further downstream, significantly reducing the duration of the flow field devoid of shock waves. Eventually, the oblique shock train persists above the combustor, marking the transition into the dual combustion mode. Consequently, the flame gradually flattens and transitions to the shear-layer stabilization.

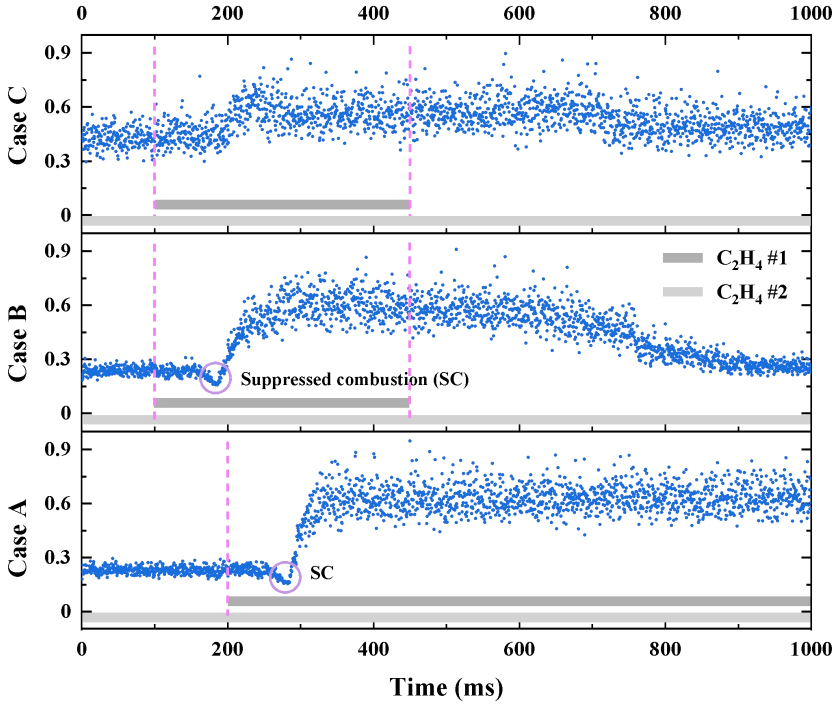


**Fig. 6** The normalized instantaneous change curves of flame intensity under different working conditions. The gray rectangular patterns indicate the opening and closing time of the two fuel pipelines. Within the purple circle, the time when combustion is suppressed is identified.

The spontaneous emission image was subjected to rigorous data processing, enabling the extraction of flame intensity values at various time points. As evident from Fig. 6, there are significant changes in flame intensity before and after the combustion mode transition. Specifically, during the supersonic-to-dual and dual-to-subsonic transitions, an increase in flame intensity is observed. Conversely, during the subsonic-to-dual and dual-to-supersonic transitions, a decrease is noted. The valve of the fuel supply pipeline was opened, and after a brief delay, the $C_2H_4$ #1 pipeline began to inject fuel. The flame intensity did not increase straight away, but decreased initially and then increased, which was particularly evident during the supersonic-to-dual transition. This could be due to the added fuel absorbing heat upon entering the combustor, thereby suppressing the combustion and causing the flame intensity to decrease. Once the added fuel was ignited, the combustion intensified and the flame intensity rose.

## 4. Summary and conclusions

In conclusion, the mode transition process of a cavity-based scramjet was investigated using high-speed schlieren and CH* spontaneous emission imaging. The combustion flow field structure images and dynamic evolution throughout the four distinct mode transition processes were captured. Based on the observed shock wave structure, flame morphology, and heat release distribution during the

mode transition, the various mode transition processes into distinct phases were categorized. The primary conclusions drawn from this analysis are as follows:

(1) Significant disparities exist in the flow field structure and heat release zone distribution within the combustor under varying combustion modes. As the mode transition process takes place, the fuel flow undergoes alterations, leading to substantial changes in the heat release characteristics of the combustor. These changes subsequently influence the back pressure within the combustor, further impacting the shock wave structure. Notably, structural oscillations of the flame and shock wave are prominent during the mode transition process.

(2) The supersonic-to-subsonic mode transition process can be systematically categorized into five distinct phases. First, the first reflected shock wave progresses forward and shortens, accompanied by flame enhancement. Second, both reflected shock waves move forward, with their inter-distance narrowing, and the flame expands into the cavity. Third, the oblique shock wave intersects with the reflected shock wave, initiating the formation of an oblique shock train. Fourth, the oblique shock train oscillates forward, leading to repeated transitions between the dual combustion mode and the subsonic combustion mode. Ultimately, due to the escalating heat release, the shock train is propelled towards the isolator, stabilizing the combustor in the subsonic combustion mode.

(3) The dual-to-supersonic transition process can be categorized into three distinct phases. First, the intensity of the oblique shock train diminishes, with occasional appearance of a strong oblique shock wave upstream of the injection that dissipates rapidly. The flame is characterized as a jet-wake stabilization. Second, the duration of the oblique shock wave increases. The flame transitions to a combined cavity shear-layer/recirculation stabilization. Finally, the oblique shock wave is strengthened and extends to the top of the combustor, forming a reflected shock wave. This marks the transition of the combustor into the supersonic combustion mode. And the flame settles into a shear-layer flame stabilization.

(4) The alteration of the flow field structure during the subsonic-to-dual transition process can be delineated into two phases. In the initial phase, the oscillation amplitude of the oblique shock train remains small, with the shock train occasionally manifesting in the upper left corner of the combustor. The flame is mainly manifested in jet-wake stabilization. In the subsequent phase, the heat release weakens further, resulting in an extension of the duration for which the oblique shock train remains. Additionally, the backward distance is increased. Notably, the back pressure is insufficient to expel the shock train from the combustor, thereby resulting in the transition to the dual combustion mode.

## Acknowledgments

This work is supported by the National Natural Science Foundation of China (NSFC) (Nos. 12322211, 11925207, 12172379, 92252206) and the Youth Independent Innovation Science Found Project of the National University of Defense Technology (No. ZK23-40).

## References

1. Ding, Y.B., Yue, X.K., Chen, G.S., et al.: Review of control and guidance technology on hypersonic vehicle. Chin. J. Aeronaut. 35(7), 1-18 (2022)
2. Luo, T.G., Zhu, J.J., Sun, M.B., et al.: MCGA-assisted ignition process and flame propagation of a scramjet at Mach 2.0. Chin. J. Aeronaut. 36(7), 378-387 (2023)
3. Feng, R., Zhu, J.J., Wang, Z.G., et al.: Ignition modes of a cavity-based scramjet combustor by a gliding arc plasma. Energy 214, 118875 (2021)
4. Wang, Z.G.: Flame stability and propagation in supersonic flow. Science Press, BeiJing (2015)
5. Sun, M.B., Wang, Z.G., Liang, J.H., et al.: Flame characteristics in supersonic combustor with hydrogen injection upstream of cavity flameholder. J. Propul. Power 24(4), 688-696 (2008)
6. Mathur, T., Gruber, M., Jackson, K., et al.: Supersonic combustion experiments with a cavity-based fuel injector. J. Propul. Power 17 (6), 1305-1312 (2001)

7. Wang, Z.P.: Studies on Mode Transition Mechanism and Operation Characteristics in a Supersonic Combustor. University of Chinese Academy of Sciences (2016)
8. Mitani, T., Hiraiwa, T., Sato, S., et al.: Comparison of scramjet engine performance in Mach 6 vitiated and storage-heated air. J. Propul. Power 13(5), 635-642 (1997)
9. Chun, J., Scheuermann, T., Von, W.J., et al.: Experimental study on combustion mode transition in a scramjet with parallel injection. 14th AIAA/AHI Space Planes and Hypersonic Systems and Technologies Conference. Canberra, Australia (2006)
10. Takahashi, S., Yamano, G., Wakai, K., et al.: Self-ignition and transition to flame-holding in a rectangular scramjet combustor with a backward step. Proc. Combust. Inst. 28(1), 705-712 (2000)
11. Takahashi, S., Demise, S., Oshita, M., et al.: Correlation between heat flux distribution and combustion mode in a scramjet combustor. ISABE (2001)
12. Takahashi, S., Tanaka, H., Noborio, D., et al.: Mach 2 supersonic combustion with hydro-carbon fuels in a rectangular scramjet combustor. ISABE (2003)
13. Kobayashi, K., Tomioka, S., Kato, K., et al.: Performance of a dual-mode combustor with multistaged fuel injection. J. Propul. Power 22(3), 518-526 (2006)
14. Li, F., Wang, Z.P., Yue X.L., et al.: Experimental study on judgment method of combustion mode on dual-mode scramjet. Chinese Joural of Theoretical and Applied Mechanics 47(3), 389-397 (2015)
15. Wang, H.B., Wang, Z.G., Sun, M.B., et al. Combustion modes of hydrogen jet combustion in a cavity-based supersonic combustor. Int. J. Hydrogen Energy 38(27), 12078-12089 (2013)
16. Sullins, G.A.: Demonstration of Mode Transition in a Scramjet Combustor. J. Propul. Power 9(4), 515-520 (1993)
17. Fotia, M.L., Driscoll, J.F.: Ram-scram transition and flame/shock-train interactions in a model scramjet experiment. J. Propul. Power 29(1), 261-273 (2013)
18. Zhou, R.X., Meng, F.Z., Li, T., et al.: Ram to scram mode transition in a simulated flight acceleration. Phys. Fluids 34(6), 1-16 (2022)
19. Aguilera, C., Yu, K.H.: Scramjet to ramjet transition in a dual-mode combustor with fin-guided injection. Proc. Combust. Inst. 36(2), 2911-2918 (2017)
20. Lian, H., Gu, H.B., Zhou, R.X., et al.: Investigation of mode transition and thrust performance in transient acceleration and deceleration experiments. Journal of Experiments in Fluid Mechanics 35(1), 97-108 (2021)
21. Zhang, X., Zhang, Q.F., Wu, Z.J., et al.: Experimental study of hysteresis and catastrophe in a cavity-based scramjet combustor. Chin. J. Aeronaut. 35(10), 118-133 (2021)
22. Tian, L., Chen, L.H., Chen, Q., et al.: Quasi-one-dimensional multimodes analysis for dual-mode scramjet. J. Propul. Power 30(6), 1559-1567 (2014)